Supplementary information

A bi-component supramolecular gel for selective fluorescent detection and removal of Hg^{2+} in water

Hai-Long Yang[a], Xiao-Wen Sun[a], You-Ming Zhang[a,b]*, Zhong-Hui Wang[a], Wei-Zhu[a], Yan-Qing Fan[a], Tai-Bao Wei[a], Hong Yao[a] and Qi Lin[a]*

[a] *Research Center of Gansu Military and Civilian Integration Advanced Structural Materials; College of Chemistry and Chemical Engineering, Northwest Normal University, Lanzhou, Gansu, 730070, P. R. China*

[b] *College of Chemistry and Chemical Engineering, Lanzhou City University, Lanzhou, Gansu, 730070, P. R. China*

* *Corresponding author.*

E-mail addresses: zhangnwnu@126.com (Y.-M. Zhang), linqi2004@126.com (Q. Lin).

Table of Contents

Synthesis of compound **R** and **Q**

(1) The **R** was synthesized according to previous reports [S1].

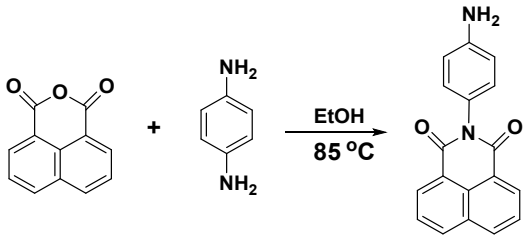

Scheme S1 The synthesis of the **R**.

The **R** was synthesized according to literature method. A mixture of the *p*-phenylenediamine (5 mmol, 0.99 g), 1, 8- naphthalic anhydride (5 mmol, 0.99 g) in ethanol (50 mL) were was stirred at 85 ˚C for 24 h. After cooling to room temperature, the precipitate was filtered, then with ethanol recrystallization get yellow powder product **R** (1.30 g, 90%, yield); M.P.:＞250 ˚C. ^{1}H NMR (400 MHz, DMSO-d_6, room temperature) δ (ppm): 8.50-8.47 (m, 4H), 7.91-7.87 (t, J = 7.8 Hz, 2H), 6.96-6.94 (d, J = 8.6 Hz, 2H), 6.66-6.64 (d, J = 8.6 Hz, 2H), 5.27 (s, 2H). ^{13}C NMR (DMSO-d_6, 150 MHz): ^{13}C NMR (DMSO-d_6, 150 MHz): 164.35, 148.97, 134.61, 131.79, 131.07, 129.62, 128.09, 127.58, 124.23, 123.10, 114.16. ESI-MS m/z: Calcd for $C_{18}H_{12}N_2O_2$, [**M** + Na]$^{+}$: 311.0791; found 311.0794.

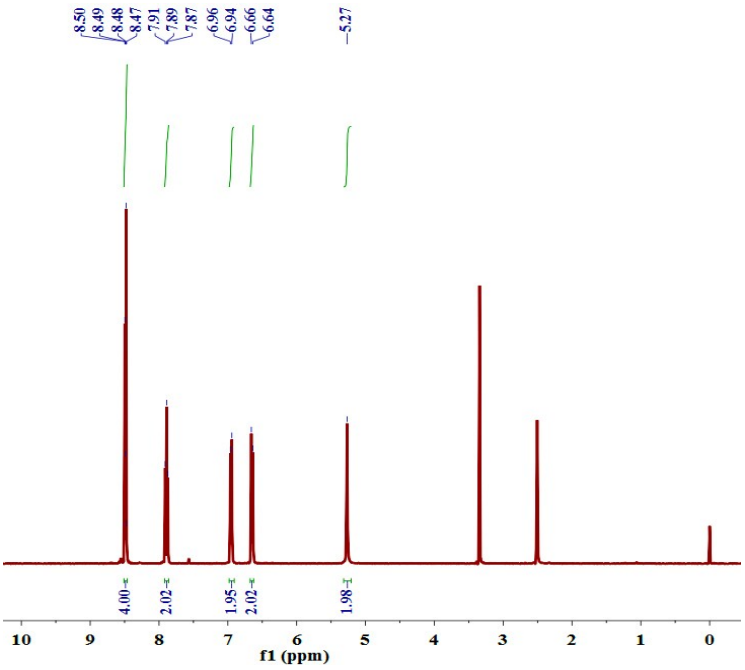

Fig. S1 ^{1}H NMR spectrum of the **R** in DMSO-d_6.

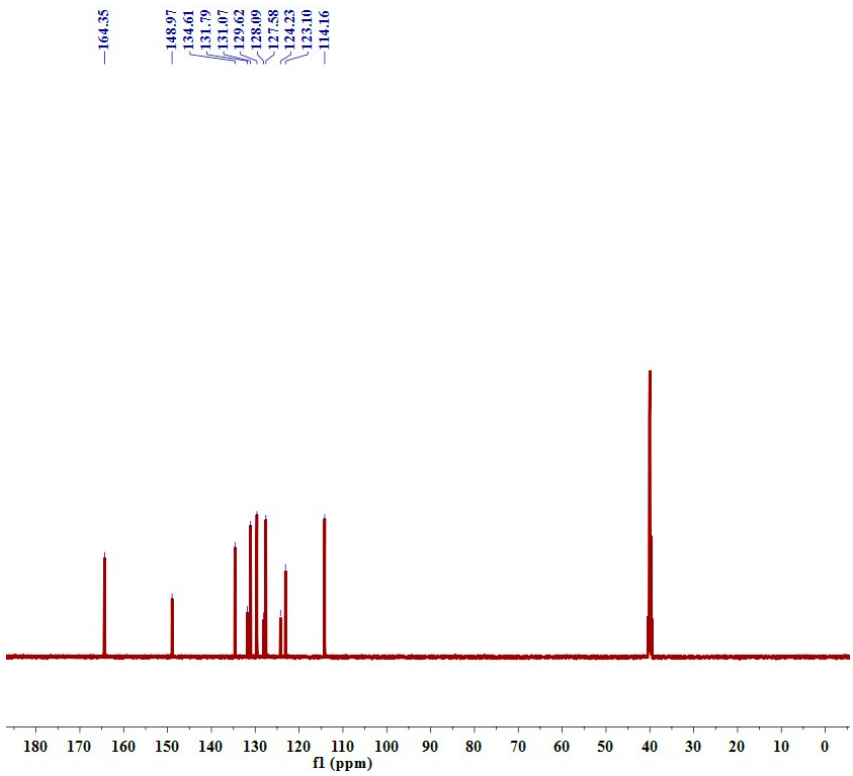

Fig. S2 ^{13}C NMR spectrum of the **R** in DMSO-d_6.

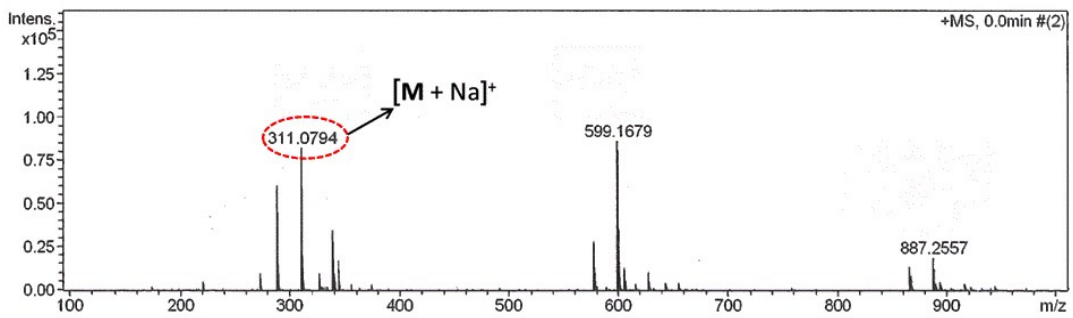

Fig. S3 ESI-MS spectrum of the **R**.

(2) The **Q** was synthesized according to previous reports [S2].

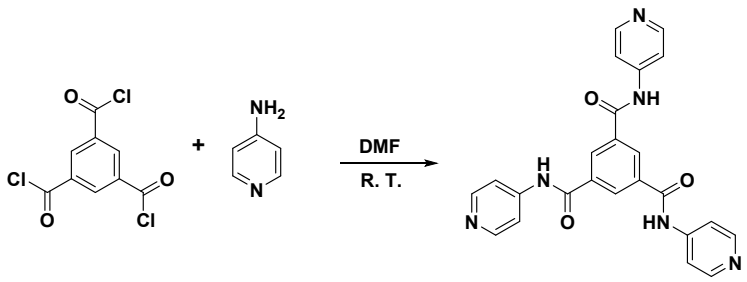

Scheme S2 The synthesis of the **Q**.

A 20 mL DMF containing 10 mmol (2.64 g) of the 1, 3, 5-benzene-tricarbonyl

trichloride was added drop by drop to a 40 mL DMF solution containing 30.5 mmol (2.86 g) of the 4-aminopyridine and 35mmol (4.8 mL) of the distilled triethylamine at 0 ˚C with continuous stirring. After stirred for 12 h, the reaction temperature was allowed to rise to room temperature. The resulted product was recrystallized from a mixed solvent of DMSO (100 mL) and H_2O (200 mL) and dried at 80 ˚C under vacuum (3.50 g, 80%, yield); M.P.: 167-170 ˚C. ^{1}H NMR (400 MHz, DMSO-d_6, room temperature) δ/ppm: 11.78 (s, 3 H), 8.99 (s, 3 H), 8.67 (s, 6 H), 8.26-8.19 (m, 6 H). ^{13}C NMR (DMSO-d_6, 150MHz): 165.68, 156.37, 149.58, 135.07, 131.36, 114.75. ESI-MS m/z: Calcd for $C_{24}H_{18}N_6O_3$, [**Q** + H]$^+$: 439.1513; found 439.1507.

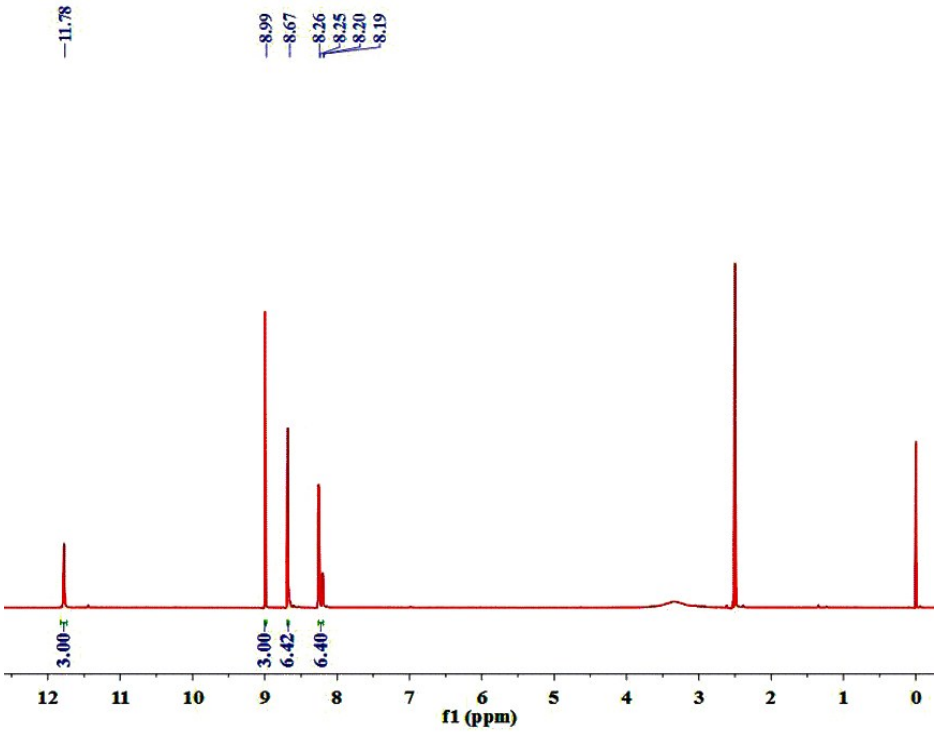

Fig. S4 ^{1}H NMR spectrum of the **Q** in DMSO-d_6.

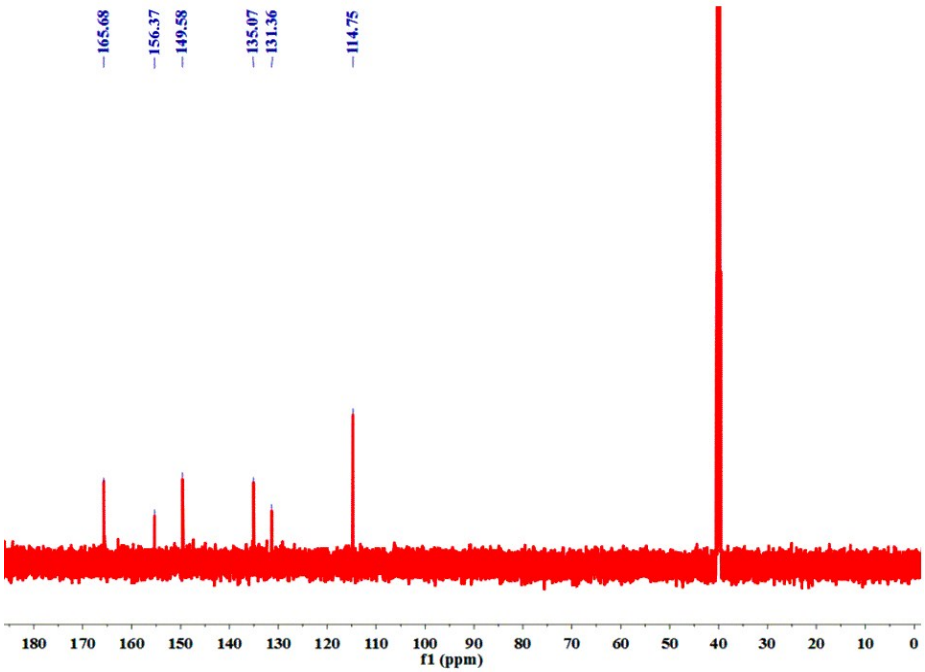

Fig. S5 ^{13}C NMR spectrum of the **Q** in DMSO-d_6.

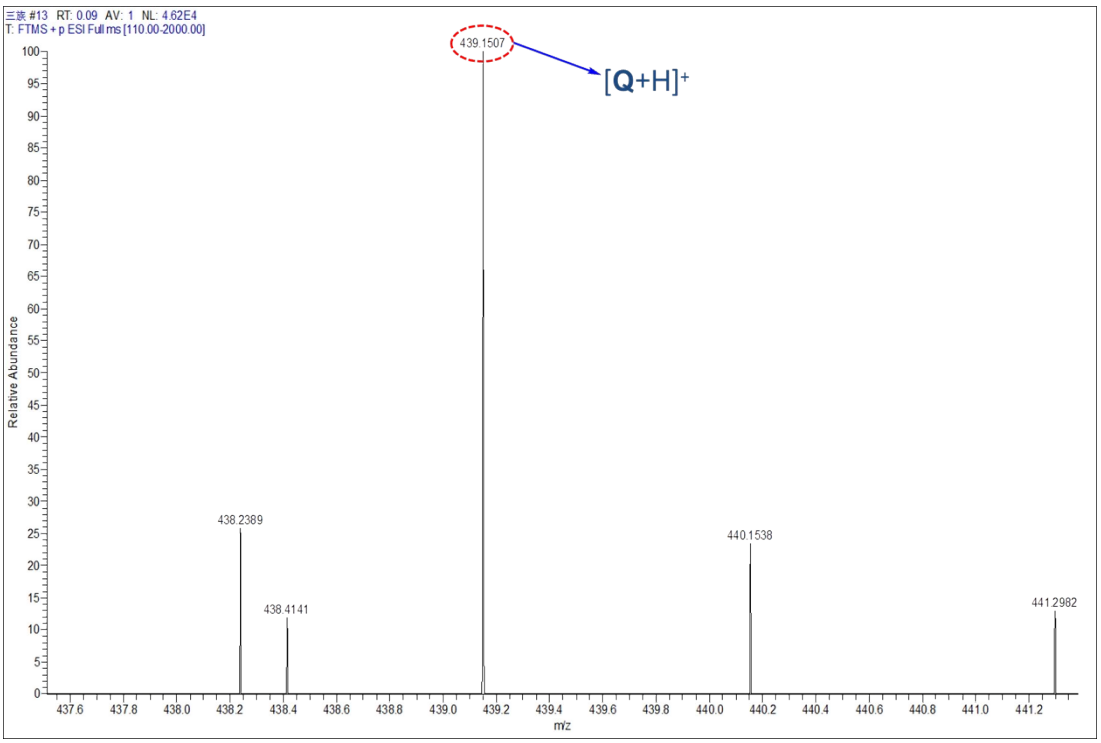

Fig. S6 ESI-MS spectrum of the **Q**.

Table S1. Gelation properties of the supramolecular gel **RQ**.

Entry	Solvent	State[a]	CGC[b](%)	Tgel[c] (℃, wt%)
1	water	P	\	\
2	acetone	P	\	\
3	methanol	P	\	\
4	ethanol	P	\	\
5	isopropanol	P	\	\
6	isopentanol	P	\	\
7	acetonitrile	P	\	\
8	THF	P	\	\
9	DMF	S	\	\
10	DMF-H_2O	G	5	85(5%)
11	DMSO	S	\	\
12	DMSO-H_2O	G	3.5	90(3.5%)
13	ethanediol	P	\	\
14	benzene	P	\	\
15	CH_2Cl_2	P	\	\
16	$CHCl_3$	P	\	\
17	CH_2ClCH_2Cl	P	\	\
18	petroleum ether	P	\	\
19	ethyl acetate	P	\	\
20	n-propanol	P	\	\
21	n-butyl alcohol	P	\	\
22	n-amyl alcohol	P	\	\
23	cyclohexanol	P	\	\
24	n-hexanol	P	\	\
25	CCl_4	P	\	\

[a]G, P and S denote gelation, precipitation and solution, respectively.

[b]The critical gelation concentration (wt%, 10 mg/ml = 1.0%).

cThe gelation temperature (℃).

Table S2. Optimum water content of gelation conditions

Entry	Water solvent	State[a]	Tgel[c] (℃, wt%)
1	0%	S	\
2	5%	S	\
3	10%	S	\
4	15%	P	\
5	20%	P	\
6	25%	P	\
7	30%	P	\
8	35%	G	70
9	39%	G	90
11	45%	G	75
12	50%	G	70

[a]G, P and S denote gelation, precipitation and solution, respectively.

[b]The critical gelation concentration (wt%, 10 mg/ml = 1.0%).

[c]The gelation temperature (℃).

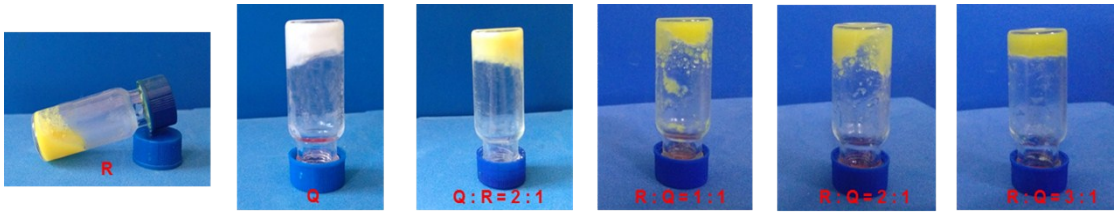

Fig. S7. Photograph of gelling ability of the **R** and **Q** at different ratios.

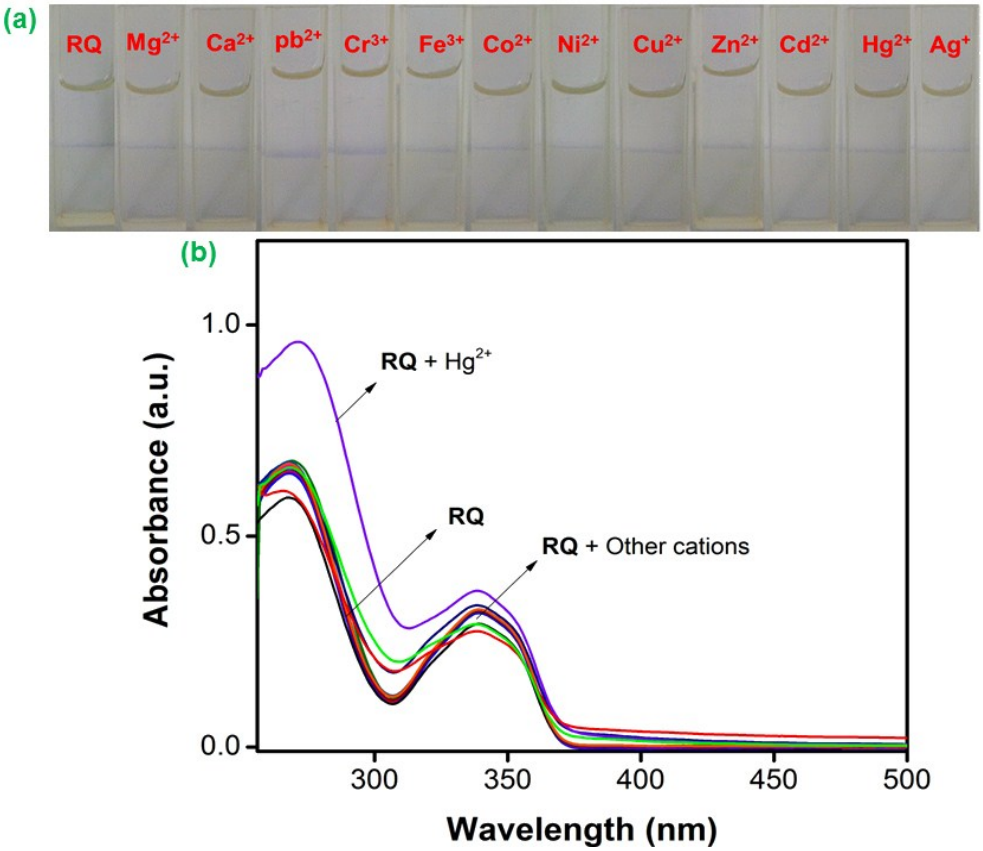

Fig. S8. (a) Natural photos and (b) UV-vis spectra responses of the supramolecular gel **RQ** (DMSO-H_2O (6.1 : 3.9, v/v)) upon adding of various metal ions (Mg^{2+}, Ca^{2+}, Pb^{2+}, Cr^{3+}, Fe^{3+}, Co^{2+}, Ni^{2+}, Cu^{2+}, Zn^{2+}, Cd^{2+}, Hg^{2+} and Ag^{+}).

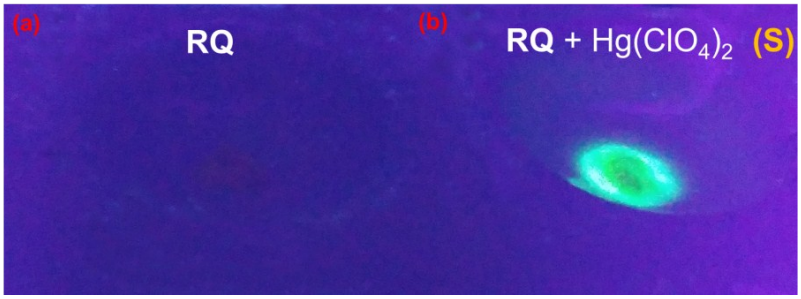

Fig. S9. Fluorescent responses of the (a) **RQ**, (b) **RQ** + $Hg(ClO_4)_2$ solid sample.

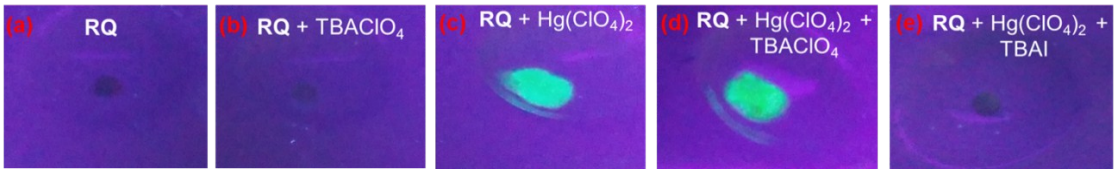

Fig. S10. Fluorescent responses of the (a) **RQ**, (b) **RQ** + $TBAClO_4$, (c) **RQ** + $Hg(ClO_4)_2$, (d) **RQ** + $Hg(ClO_4)_2$ + $TBAClO_4$ and (e) **RQ** + $Hg(ClO_4)_2$ + TBAI.

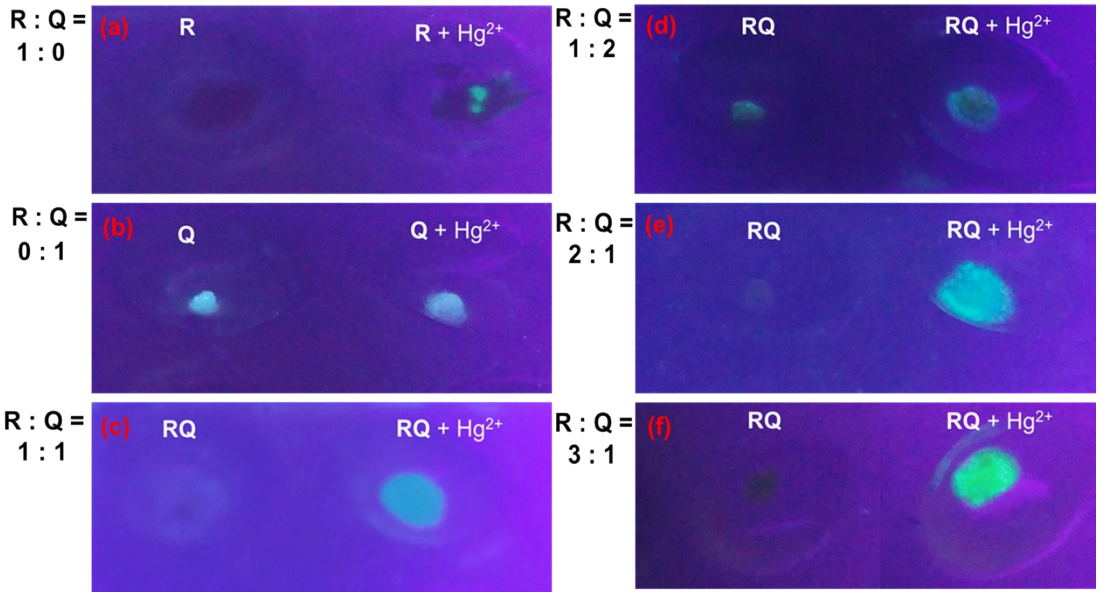

Fig. S11. Fluorescence response photos of the **RQ** and Hg^{2+} at different ratios.

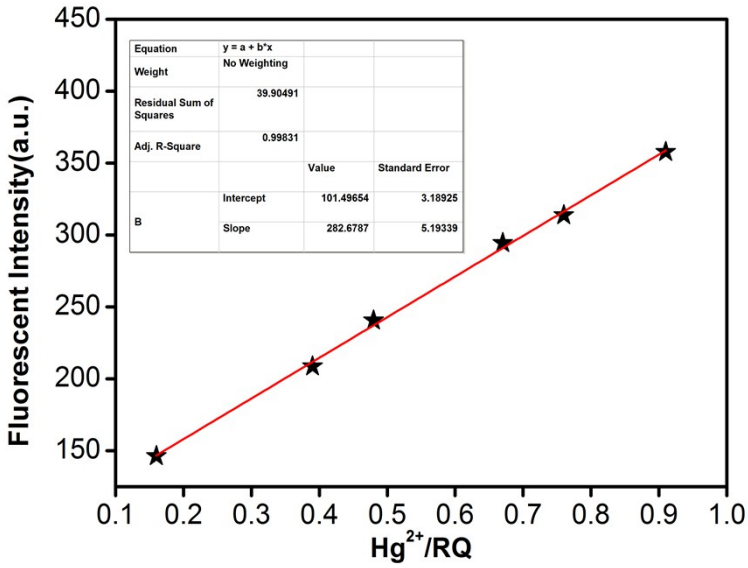

Linear Equation: Y=282.6787X + 101.49654 R^2 = 0.99831

$$\delta = \sqrt{\frac{\sum_{i=1}^{n}(X_i - \overline{X})^2}{n-1}}$$

= **4.260** **K = 3**

LOD = K×δ/s = 4.52×10^{-8} M.

Fig. S12. The photograph of the linear range.

Table S3 Comparison of the limit of lowest detection of the Hg^{2+}-sensor with previously reported Hg^{2+} sensor

No.	Journal, Year, Volume, Page	State	LOD (M)	Adsorption removal rate (%)
1	Talanta, 2014, 118, 111-117	S	5.0×10^{-8}	—
2	Anal. Chem., 2015, 87, 5148-5155	S	1.0×10^{-6}	—
3	Sen. Actuators B, 2015, 220 381-388	S	5.56×10^{-7}	—
4	Sen. Actuators B, 2016, 226, 332-341	S	2.36×10^{-6}	—
5	New J. Chem., 2017, 41, 3303-3307	S	1.785×10^{-7}	—
6	Sen. Actuators B, 2017, 238, 166-174	S	4.79×10^{-7}	—
7	Chem. Select, 2018, 3, 2088-2091	S	1.70×10^{-6}	—
8	Inorg. Chem., 2018, 57, 120-128	S	1.50×10^{-7}	—
9	J. Agric. Food Chem., 2018, 66, 6188-6195	S	6.0×10^{-8}	—
10	Anal. Methods, 2019, 11, 1879-1883	S	1.60×10^{-7}	—
11	J. Am. Chem. Soc., 2019, 141, 4756-4763	S	3.0×10^{-7}	90
12	This work	G	4.52×10^{-8}	91

G and **S** denote gelation and solution, respectively

Table S4 The ICP date of xerogel **RQ** for Hg^{2+}

Ion	Initial concentration (mg/L)	Residual concentration (mg/L)	Adsorption removal rate (%)
Hg^{2+}	20.1	1.78	91.14

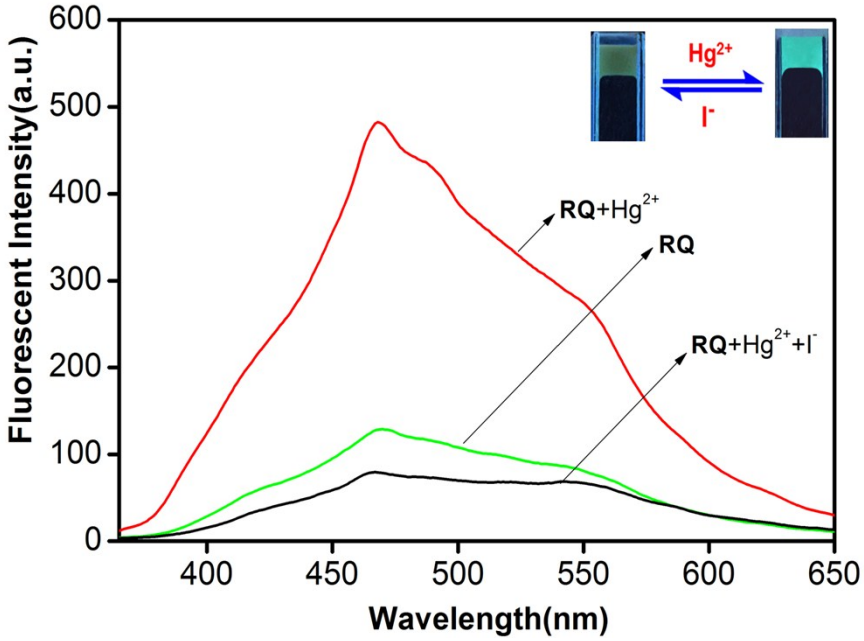

Fig. S13. Fluorescence spectra of the **RQ**, **RQ** + Hg^{2+} and **RQ** + Hg^{2+} + I^{-}.

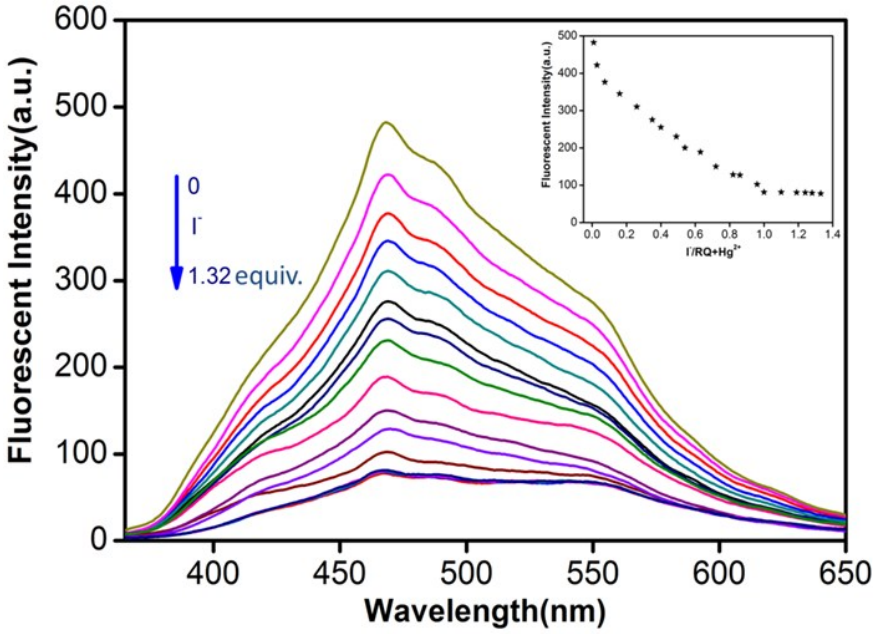

Fig. S14. Fluorescence spectra of the **RQ** + Hg^{2+} in the presence of different concentrations of aqueous I^{-} and fluorescence changes at 460 nm.

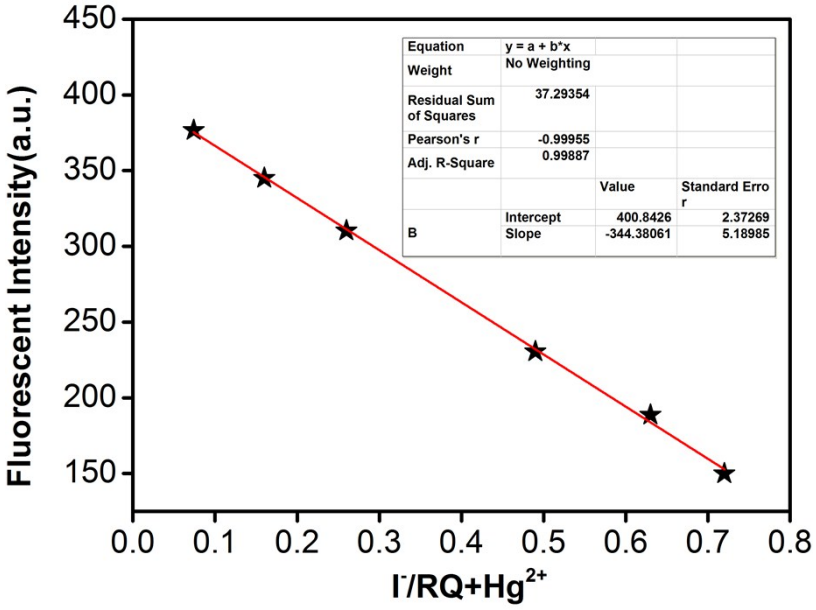

Linear Equation: Y= -344.38061X + 400.8426 R^2 = 0.99887

= 4.248 K = 3

LOD = K δ/s = 3.70 10^{-8} M.

Fig. S15. The photograph of the linear range.

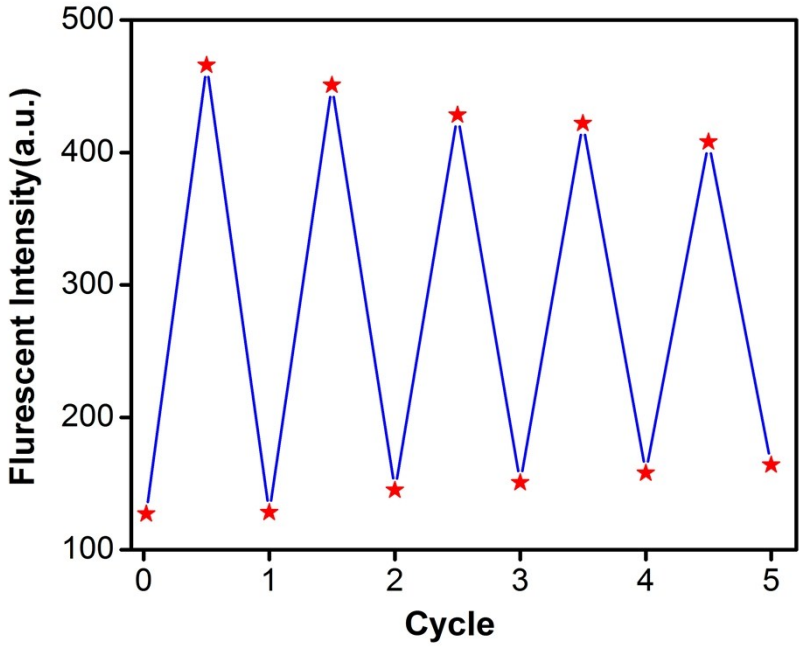

Fig. S16. The changes of fluorescent intensity "OFF-ON-OFF" cycles of the **RQ**, controlled by the alternative addition of Hg^{2+} and I^{-}.

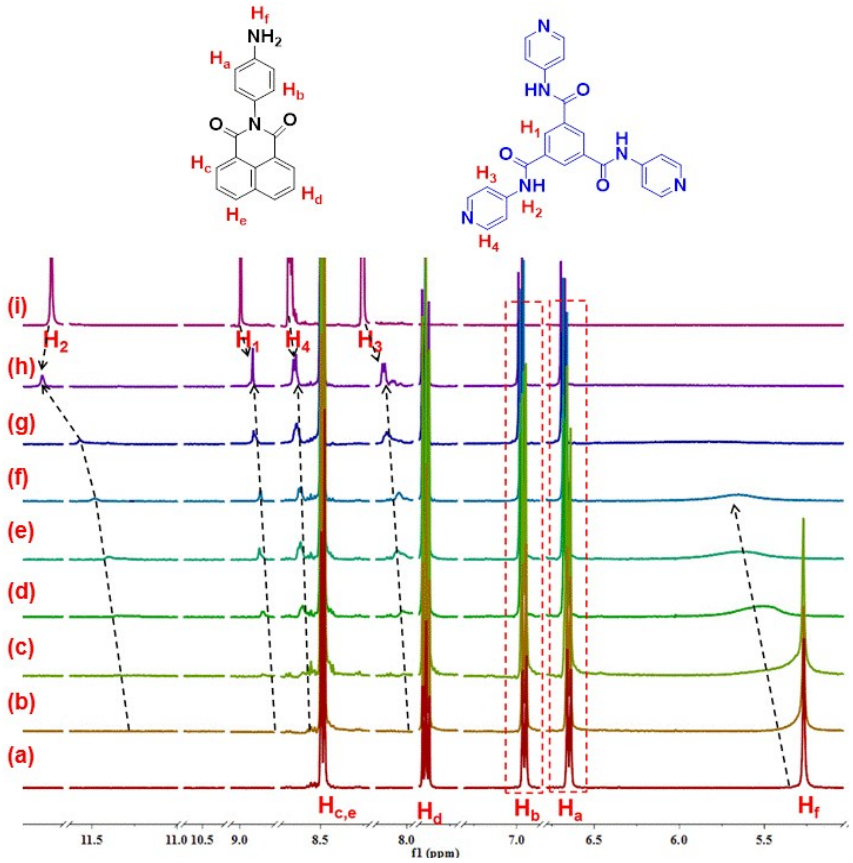

Fig. S17. The partial ^{1}H NMR spectra of the **R** in DMSO-d_6 with **Q** [(a) Free **R**; (b) ~ (h) with **Q** (0.2, 0.5, 1.0, 1.5, 2.0, 2.5 and 3.0 equiv.); (i) Free **Q**].

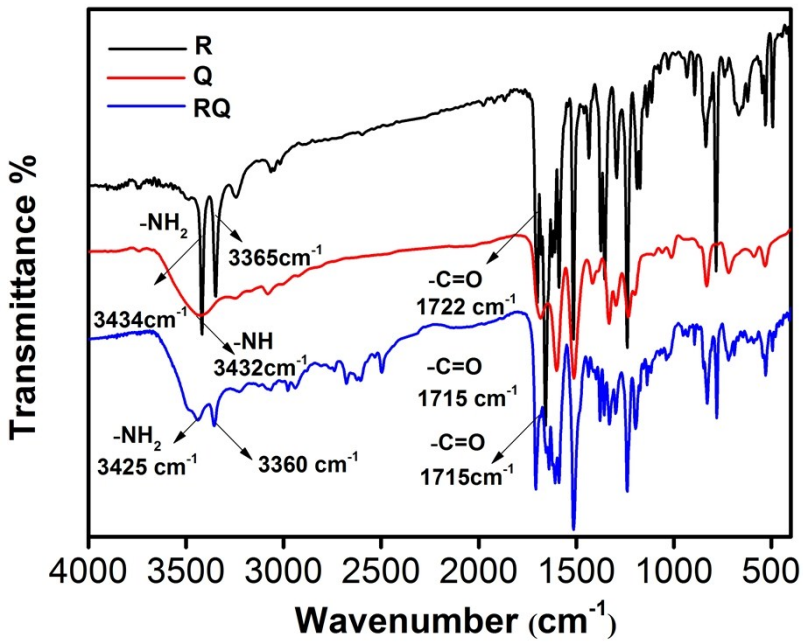

Fig. S18. IR spectra of the **Q** (red), **R** (black) and **RQ** (blue) in KBr disks.

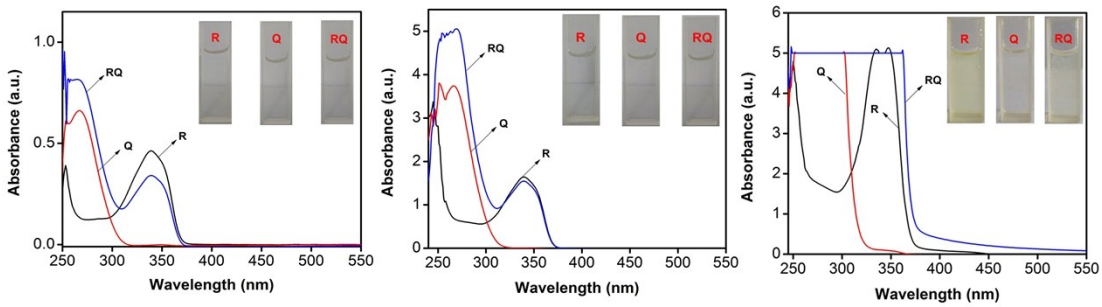

Fig. S19. The UV-vis spectra and natural photos of the **R**, **Q** and **RQ** ((a) 2.0 × 10^{-5} M; (b) 2.0 × 10^{-4} M; (c) 2.0 × 10^{-3} M).

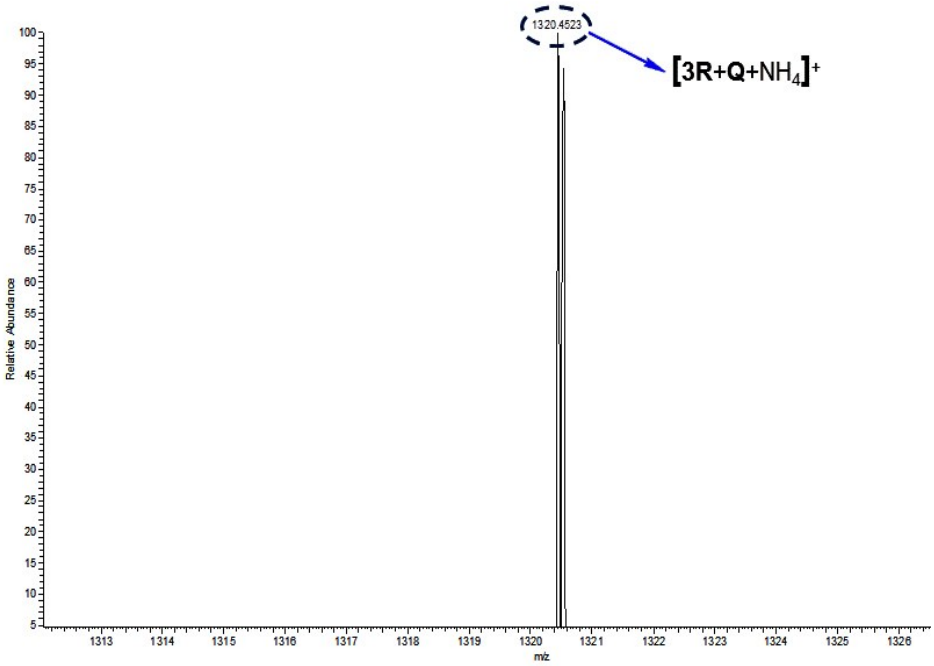

Fig. S20. Mass spectrum of the **RQ**.

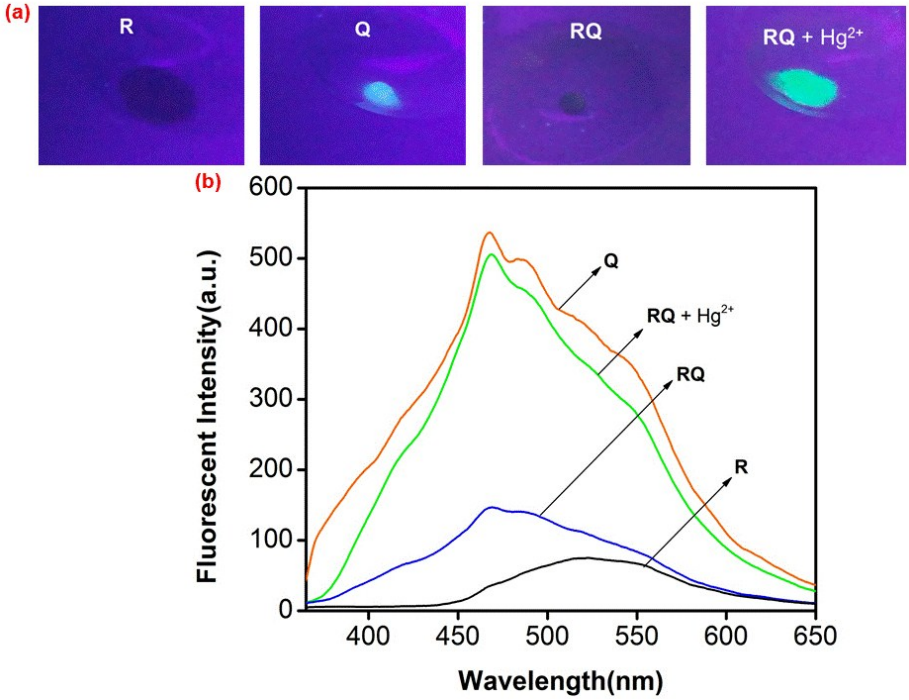

Fig. S21. (a) Fluorescent photos and (b) fluorescence spectra responses of the **R**, **Q**, **RQ** and **RQ** + Hg^{2+} (DMSO-H_2O (6.1 : 3.9, v/v) binary solution).

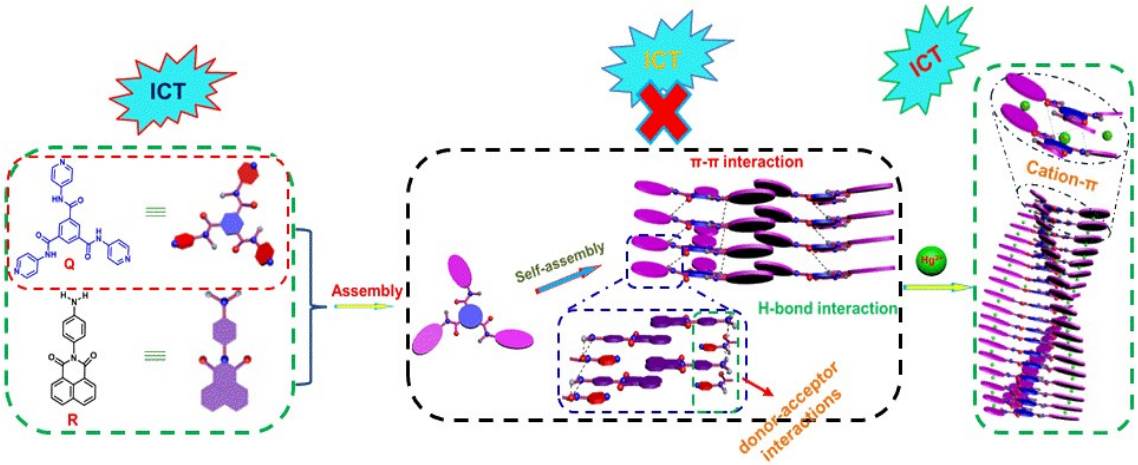

Fig. S22. The possible ICT processes during **RQ** assembly and Hg^{2+} response.

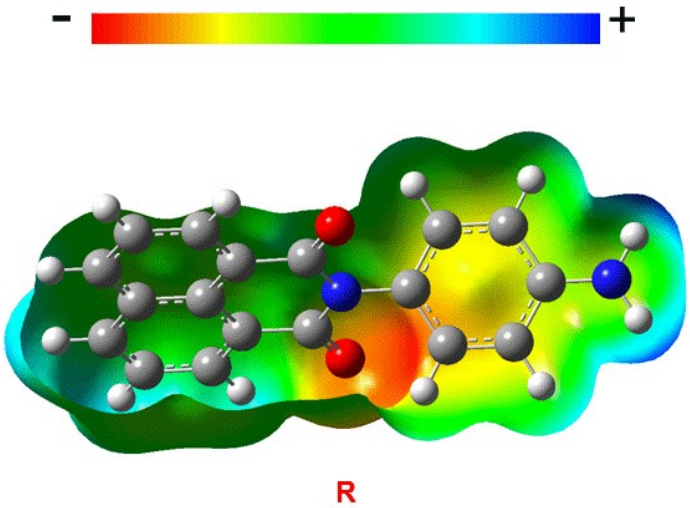

Fig. S23. ESP maps of the **R** is calculated at the B3LYP/6-31G level of theory.

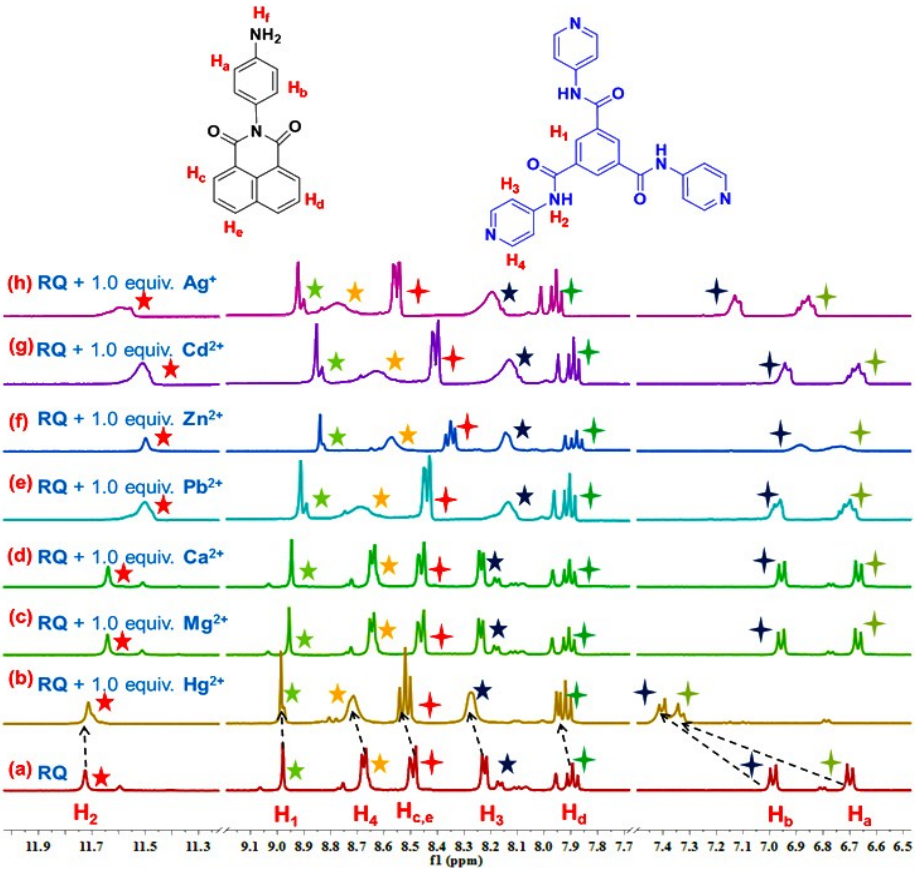

Fig. S24. ^{1}H NMR spectra of the (a) **RQ** and (b) **RQ** + Hg^{2+}, (c) **RQ** + Mg^{2+}, (d) **RQ** + Ca^{2+}, (e) **RQ** + Pb^{2+}, (f) **RQ** + Zn^{2+}, (g) **RQ** + Cd^{2+}, (h) **RQ** + Ag^{+}.

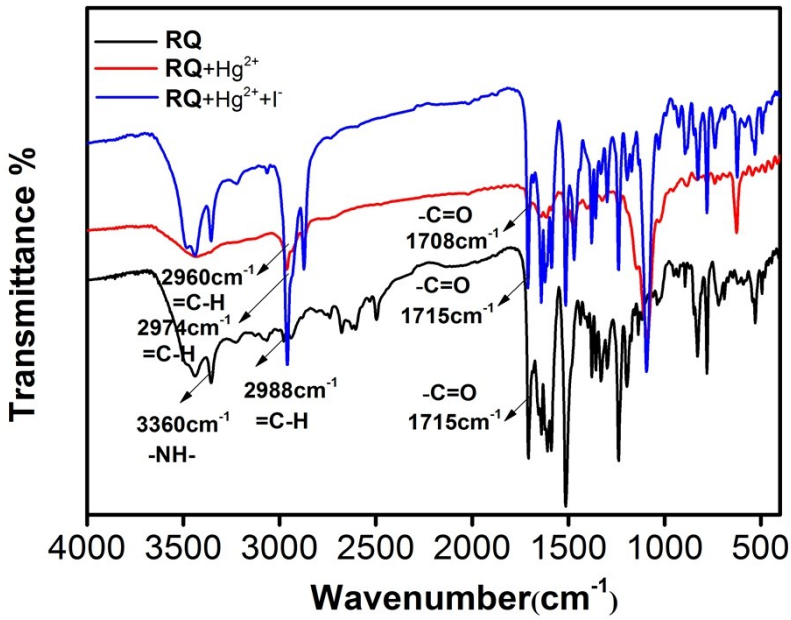

Fig. S25. IR spectra of the **RQ** (black), **RQ** + Hg^{2+} (red) and **RQ** + Hg^{2+} + I^{-} (blue) in KBr disks.

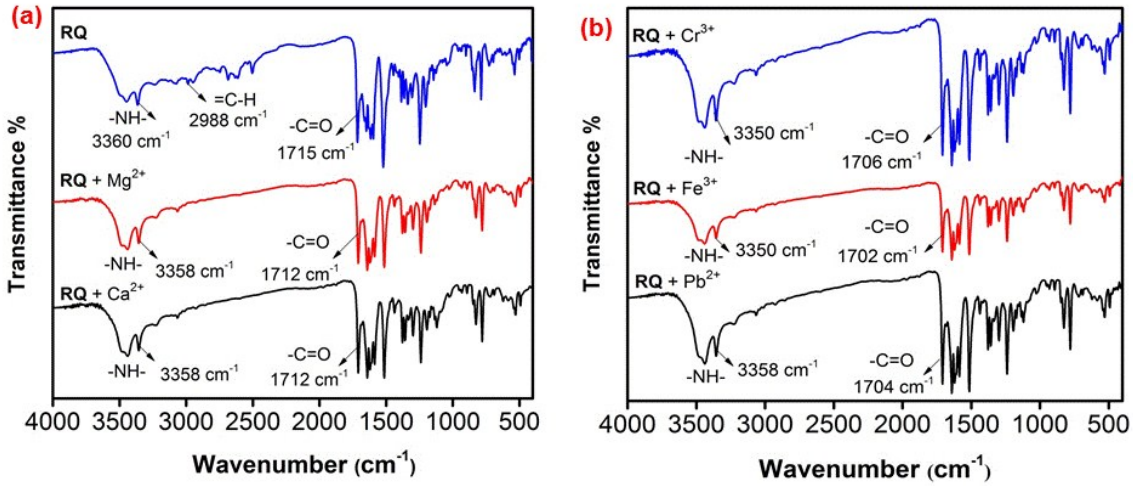

Fig. S26. (a) IR spectra of the **RQ** + Ca^{2+} (black), **RQ** + Mg^{2+} (red) and **RQ** (blue) in KBr disks; (b) IR spectra of the **RQ** + Pb^{2+} (black), **RQ** + Fe^{3+} (red) and **RQ** + Cr^{3+} (blue) in KBr disks.

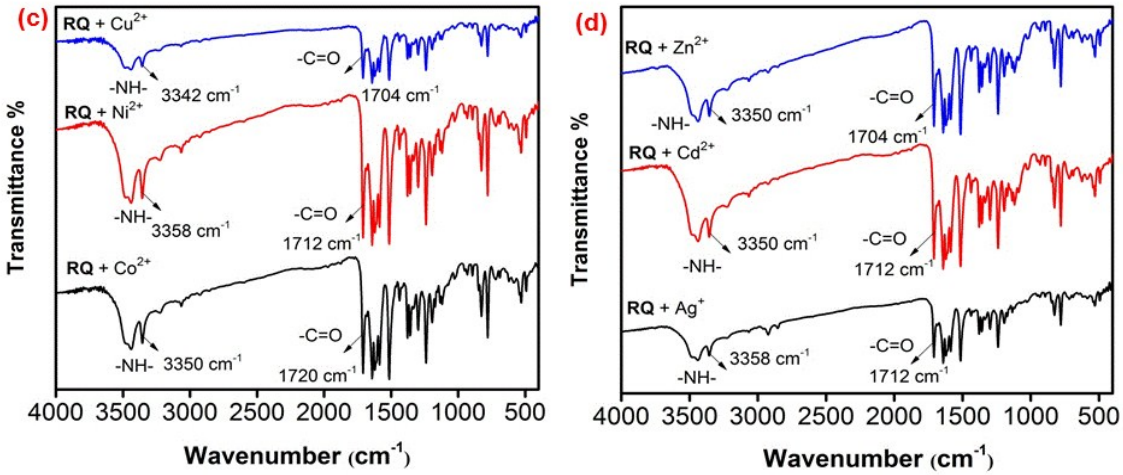

Fig. S27. (c) IR spectra of the **RQ** + Co^{2+} (black), **RQ** + Ni^{2+} (red) and **RQ** + Cu^{2+} (blue) in KBr disks; (d) IR spectra of the **RQ** + Ag^{+} (black), **RQ** + Cd^{2+} (red) and **RQ** + Zn^{2+} (blue) in KBr disks.

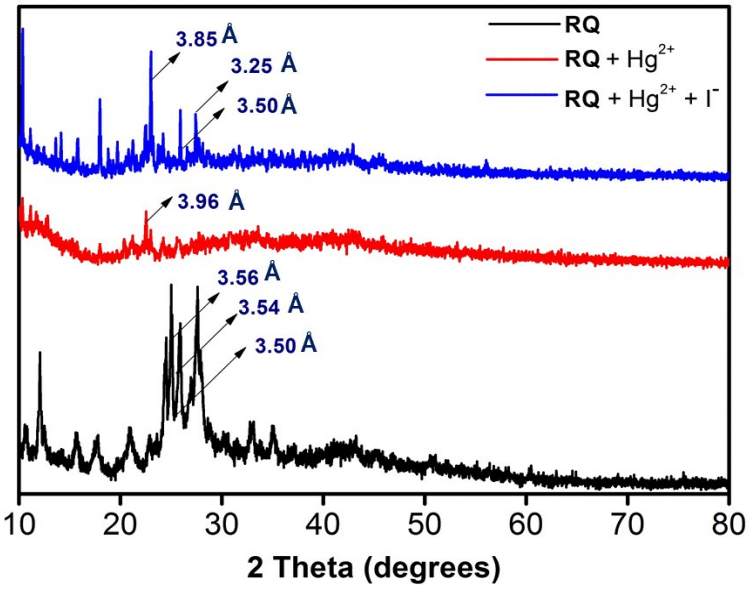

Fig. S28. Powder XRD patterns of xerogel **RQ, RQ** + Hg^{2+} and **RQ +** Hg^{2+} + I^{-}.

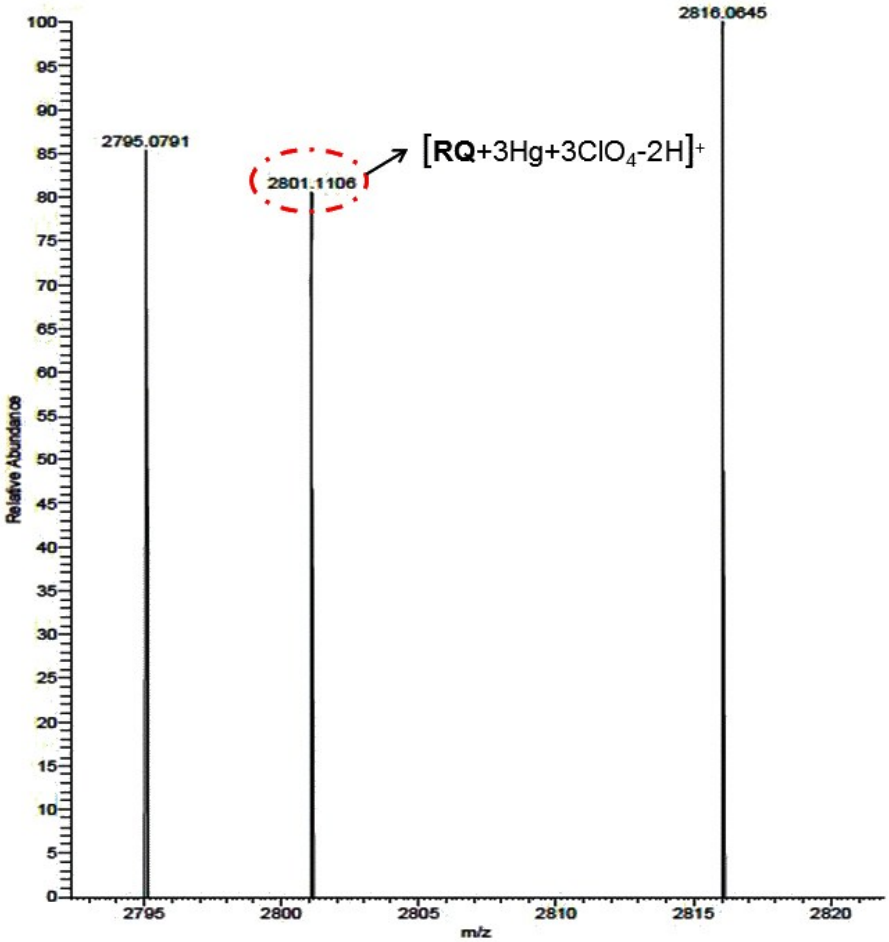

Fig. S29. Mass spectrum of the **RQ** + Hg^{2+}.

Notes and references

S1 Y. M. Zhang, B. B. Han, Q. Lin, P. P. Mao, J. F. Chen, H. Yao and T. B. Wei, *Chin. J. Org. Chem.*, 2018, **38**, 1800-1805.

S2 Y. Q. Fan, J. Liu, Y. Y. Chen, X. W. Guan, J. Wang, H. Yao, Y. M. Zhang, T. B. Wei and Q. Lin, *J. Mater. Chem. C*, 2018, **6**, 13331-13335.